SCIENCE CHINA
Chemistry

•ARTICLES•

April 2020 Vol.63 No.4: 497–503
https://doi.org/10.1007/s11426-019-9667-1

Covalent organic hollow nanospheres constructed by using AIE-active units for nitrophenol explosives detection

Shan Jiang, Shengda Liu, Lingchen Meng, Qingkai Qi, Lipeng Wang, Bin Xu, Junqiu Liu* & Wenjing Tian*

State Key Laboratory of Supramolecular Structure and Materials, Jilin University, Changchun 130000, China

Received November 8, 2019; accepted December 18, 2019; published online March 11, 2020

The development of conjugated nanomaterials with high sensitivity and super-amplified quenching effect for the detection of nitrophenol explosives is still a great challenge. Herein, we developed conjugated hollow nanospheres constructed by using aggregation-induced emission (AIE) active 1,3,5-tris(4-formyl-phenyl)benzene (TFPB). The high emission hollow nanospheres with uniform size and admirable dispersiveness exhibited obvious fluorescence quenching response with the addition of nitrophenol explosives owing to the photoinduced electron transfer (PET) from the hollow nanospheres to nitrophenol explosives. The Stern-Volmer constants of hollow spheres for 2,4,6-trinitrophenol (TNP), 4-nitrophenol (NP) and 2,4-dinitrophenol (DNP) can reach 9.67×10^5, 3.14×10^5 and 4.8×10^4 M^{-1}, respectively. Furthermore, the handy test paper coated with hollow nanospheres was prepared and showed a good response toward TNP solutions and vapor. The study provides a novel strategy to construct AIE-active conjugated hollow nanospheres for efficient nitrophenol explosives sensing.

aggregation-induced emission, covalent organic nanospheres, nitrophenol explosives detection, fluorescence quenching

Citation: Jiang S, Liu S, Meng L, Qi Q, Wang L, Xu B, Liu J, Tian W. Covalent organic hollow nanospheres constructed by using AIE-active units for nitrophenol explosives detection. *Sci China Chem*, 2020, 63: 497–503, https://doi.org/10.1007/s11426-019-9667-1

1 Introduction

Nowadays, the increasing well-organized regional terrorist bomb attacks have been heavily threatened the human social security. Additionally, the wide application of explosives in chemical plants and defense industries has also led to significant environment pollution and harmful effects on human health due to high toxicity [1–3]. Nitroaromatics explosives, such as 2,4,6-trinitrophenol (TNP), 4-nitrophenol (NP) and 2,4-dinitrophenol (DNP), are the major components of the military explosives and mines [4,5]. To reduce the risk of explosives, various sophisticated instrumental techniques such as surface enhanced Raman spectroscopy [6], nuclear quadrupole resonance [7], gas chromatography mass spectroscopy [8], and X-ray diffraction [9] have been developed to detect nitroaromatics explosives. Nevertheless, most of these techniques are complicated, expensive, and time-consuming for the practical applications [10–12]. Recently, fluorescent techniques have attracted considerable research interests, owing to their advantages of low cost, fast response, noteworthy sensitivity and simple operation [13]. Various fluorescent probes, such as metal-organic frameworks [14,15], fluorescent polymers [16,17], quantum dots [18] and organic fluorescent molecules [19] have been developed to detect nitroaromatics explosives. However, their relatively low sensibility and complex synthesis process make them difficult to be used for *in-situ* detection and vapor phase sensing of nitrophenol explosives to some extent.

As potential fluorescent probes, fluorescent conjugated polymer with amplified fluorescence signal response has been developed in recent years [20–22]. Among these probes, fluorescent conjugated polymer nanomaterials with

*Corresponding authors (email: junqiuliu@jlu.edu.cn; wjtian@jlu.edu.cn)

aggregation-induced emission (AIE) feature can be applied in explosives detection due to their high brightness, uniform dispersion, and good optical stability [23–29]. For example, Tang and co-workers [26] prepared fluorescent nanosheets by crystallization of polymers capped with a typical AIE molecule tetraphenylethene (TPE), and the nanosheets exhibited sensitive and superior specific response to TNP with the Stern-Volmer constants of 3.8×10^5 M^{-1}. Besides, they developed stable AIE polymer nanoparticles for the nitroaromatics detection with the highest Stern-Volmer constants of 1.45×10^5 M^{-1} [27–29]. In recent years, hollow micro/nanospheres with high dispersibility, low density, stable chemical properties, high specific surface area and high contact possibility were reported for numerous applications, such as sensors, lithium batteries, drug delivery and solar cells [30–42]. However, only few studies focused on applying conjugated polymer hollow micro/nanospheres for explosives detection. For instance, Liao and co-workers [39] prepared hollow microspheres based on aniline/aminocarbazole copolymers (PACs), and applied them to nitro-based explosives detection with the Stern-Volmer constants of 1.08×10^4 M^{-1}.

Considering the amplified fluorescence signal response of AIE fluorescent conjugated polymer and morphological superiority of hollow spheres, herein, we developed covalent polymer hollow nanospheres (HS) via Schiff's-base-reaction by using AIE-active 1,3,5-tris(4-formyl-phenyl)benzene (TFPB) molecule as the building block and ethylenediamine as the linker. The hollow nanospheres with uniform-sized good dispersibility and strong emission displayed highly sensitive fluorescence quenching response to nitrophenol explosives owing to the photoinduced electron transfer (PET) effect.

2 Experimental

Attention! The nitroaromatic compounds (especially TNP, DNP and NP) possess extremely explosive nature. Therefore, special care should be taken when operating with appropriate safety measurements.

2.1 Materials and methods

All the solvents were purchased by commercial approaches. Ethanol and tetrahydrofuran were used with further purification. All the other chemicals were purchased from Aladdin or Aldrich (USA), and used as received without further purification.

^{1}H nuclear magnetic resonance spectroscopy (^{1}H-NMR) spectra in solution was measured by Bruker Avance III 510 spectrometer (500 MHz, Germany) at 298 K using $CDCl_3$ as solvent and tetramethylsilane (TMS) as the internal standard (δ=0.00 ppm). The time of flight mass spectra was recorded using a Kratos MALDI-TOF mass system (UK). Fourier transform infrared (FTIR) spectra were recorded on a Vertex 80V spectrometer (Germany). The sample was grinded into powder and dried, then mixed with dried potassium bromide powder and pressed into piece. Dynamic light scattering (DLS) experiments were carried out with Malvern Instrument Zetasizer Nano ZS (UK) equipped with a He-Ne laser (633 nm, 4 mW) and an avalanche photodiode detector. The DLS measurement was recorded at 25 °C and the scattering angle was fixed at 90°. UV-Vis spectra were recorded with a Shimadzu UV-2550 spectrophotometer (Japan). Fluorescence spectroscopy was taken with a Shimadzu RF-5301 PC spectrometer. Fluorescence quantum yields were measured using absolute fluorescent quantum yield via the integrating sphere method using an Edinburgh FLS980 fluorescence spectrometer (UK). Fluorescence lifetime was investigated using time-correlated single-photon counting (TCSPC) method and collected on an Edinburgh FLS980, with an Edinburgh EPL-375 picosecond pulsed diode laser as the excitation source. Scanning electron microscope (SEM) images were recorded on scanning electron microscopy (JEOL JSM 6700F, Japan). A drop of the aqueous solution was dripped directly onto a silicon wafer and air-dried. Transmission electron microscope (TEM) images were recorded on a JEM-2100F instrument with an accelerating voltage of 200 kV. The sample was prepared by placing a drop of the stock solution on a 300-mesh, carboncoated copper grid and air-dried before measurement. Atomic force microscopy (AFM) was performed on Nanoscope III a controller (Veeco Metrology, USA) Santa Barbara, CA using tapping modetin with a SiN4 tip.

2.2 Synthesis

The monomer TFPB was synthesized by using the procedure shown in Scheme S1 (Supporting Information online). It was prepared according to the previous method with little modification and characterized by ^{1}H NMR, and mass spectroscopies (Figures S1, S2) [43]. 1,3,5-tribromobenzene (100 mg, 0.32 mmol), 4-formylphenylboronic acid (216 mg, 1.44 mmol), palladiumtetrakis (triphenylphosphine) (18 mg) and aqueous solution of potassium carbonate were reacted in tetrahydrofuran for 48 h under nitrogen. The reaction mixture was added to water and extracted with dichloromethane. Then it was dried over anhydrous $MgSO_4$ and filtered. The crude product was concentrated by rotary evaporation and purified by column chromatography to afford TFPB in 71% yield. ^{1}H NMR (500 MHz, Chloroform-d) δ 10.11 (s, 3H), 8.03 (d, J=8.2 Hz, 5H), 7.91 (s, 3H), 7.88 (d, J=8.2 Hz, 6H). ESI-MS: m/z 390.43.

Polymer hollow spheres were prepared through a Schiff base reaction. Ethylenediamine (0.9 mg, 1.5×10^{-5} mol) was

added to a solution of TFPB (3.9 mg, 1×10^{-5} mol) in ethanol (20 mL). Then the mixture was stirred for 30 min at room temperature. In addition, the method of preparing the polymer hollow nanospheres in methanol and toluene was the same as that in ethanol.

2.3 Sensing studies

The quenching efficiency can be described by the Stern-Volmer equation, $I_0/I=K_{sv}[A]+1$, where I_0 and I are the fluorescence intensities, $[A]$ is the concentration of the analyte quencher and K_{sv} is the Stern-Volmer constant. Afterward, the limit of detection (LOD) was calculated from $3\sigma/k$, where k denotes the quenching constant and σ represents standard deviation in the emission of the hollow nanospheres without nitrophenol analytes. The aliquots of the nitrophenol solution were added to the ethanol solution of polymer hollow nanospheres in an incremental fashion and the fluorescence spectra were obtained accordingly. The polymer-coated indicator paper was produced by immersing the filter paper in the solution of hollow nanospheres, and then drying them in air. The filter paper was thereafter cut into 1 cm× 1 cm pieces and then used for on-site sensing. Thereafter, the vapor phase sensing was also carried out. The TNP solid was placed for 3 d at room temperature in a sealed flask, which was kept for 30 min at 30 °C before each measurement in order to ensure the saturation of the TNP vapor in the flask.

2.4 Cyclic voltammetry studies

Cyclic voltammetry (CV) measurements were carried out using CHI 620E electrochemical workstation with three electrode system [44]. Tetrabutylammonium hexafluorophosphate (TBAPF6) in anhydrous dichloromethane (0.1 M) was used as the supporting electrolyte. Glassy carbon electrode (GCE) with 3 mm in diameter was used as the working electrode, Ag/AgCl was used as the reference electrode and platinum wire electrode was used as the counter electrode. 5 mg polymer was mixed with isopropyl alcohol (0.48 mL), subsequently added with 25 μL 5 wt% Nafion and sonicated in a bath sonicator for 1 h. 20 μL of the polymer mixture was drop casted on the Glassy carbon working electrode surface and air dried overnight. CV studies were done at room temperature and the scan rate of the electrochemical measurements was 100 mV s^{-1}.

2.5 Theoretical calculations

2.5.1 Molecular dynamics simulations

The force field is COMPASSII and the atomic charges are generated according to force field. The total energy is minimized for 50,000 steps. The particle mesh Ewald (PME) summation method was applied to treat the long range electrostatic interactions with a periodic boundary condition. The time step in all molecular dynamics (MD) simulations was 2 fs.

2.5.2 DFT calculation

First-principles density functional theory (DFT) calculations were performed using the projected augmented wave (PAW) [45]. The Perdew-Burke-Ernzerhof exchange-correlation functional of the generalized-gradient approximation (PBE-GGA) was adopted for the exchange-correlation functional [46]. In all calculations, the plane-wave expansion of the wave functions with an energy cutoff of 400 eV was applied. A vacuum region of 20 Å was inserted between the periodic slabs along the Z direction in order to avoid the interlayer interactions.

2.5.3 Molecular modelling of interactions between hollow nanosphere and TNP

Interactions between the polymer hollow nanospheres and TNP were theoretically interrogated by molecular modelling via molecular docking and MD simulation according to the Refs. [47,48]. Specifically, the repeat unit of polymer HS was built in 3D coordinates using the MOE's (molecular operating environment software package, Chemical Computing Group, Canada) builder tool. The 3D structures were preoptimized before running simulations using an Amber10 force field. Subsequently, TNP was docked into the minimized HS structures using the MOE software package to calculate the intermolecular interactions.

3 Results and discussion

3.1 Synthesis and characterization

Polymer hollow spheres were prepared by using AIE-active TFPB as the building block and ethylenediamine as the soft linker through simple synthesis method based on our previous work (Figure S3) [30]. The forming process of hollow spheres was directly observed by TEM (Figure S4). Initially, the polymer lamels were formed rapidly and then curled into hollow nanospheres. The absorption and PL spectra of hollow nanospheres were shown in Figure S5 and the PL spectra of hollow nanospheres with the change of the reaction time were shown in Figure S6. The fluorescence intensity of the polymer hollow spheres gradually increased along with the reaction time and it saturated at 30 min because the AIE-active monomer TFPB aggregated during the polymerization process until the covalent hollow nanospheres were completely emerged. To further monitor the fluorescent property before and after the polymerization process, we testified the fluorescence quantum yield of TFPB monomer and polymer hollow spheres in ethanol solution (Figure S7). As can be seen, the hollow nanospheres had higher fluorescence

quantum yield (Φ_F=7.72%) than that of isolated TFPB monomer, indicating the fluorescence enhancement of polymerization process [17,20,30]. The forming process of the fluorescent hollow nanospheres was shown in Scheme 1.

The FTIR spectroscopy (Figure S8) showed that the stretching vibration peak of C=O centered at 1674 cm^{-1} almost disappeared, while that of the C=N peaked at 1639 cm^{-1} emerged at the same time, demonstrating the formation of hollow spheres. As shown in Figure 1(a), TEM image presented spherical structures with uniform size, and the distinguishing contrast between the periphery and inner part confirmed the architecture of hollow nanospheres. Both the SEM image (Figure 1(b)) and AFM analysis (Figure 1(c)) presented that the average diameter of the hollow spheres was about 150 nm. Besides, the DLS data showed that the volume average hydrodynamic diameter of the hollow nanospheres was 169.4 nm with a narrow size distribution (Figure 1(d)).

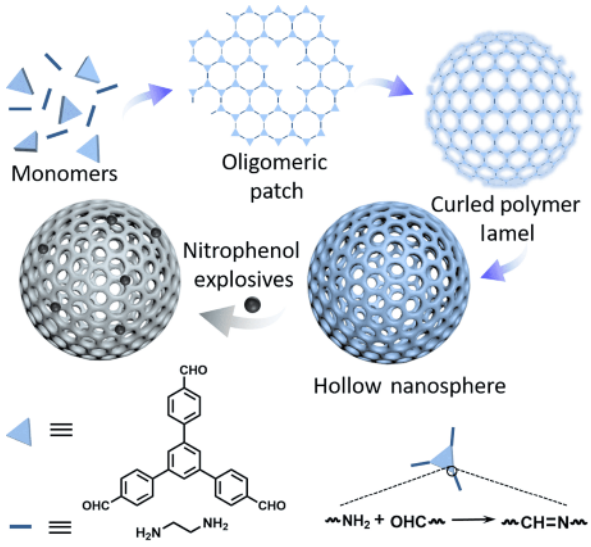

Scheme 1 Schematic representation of the forming process of the fluorescent hollow nanospheres and their application in the detection of nitrophenol explosives (color online).

3.2 Sensing for explosives in solution

We investigated the fluorescence sensing behaviors of the hollow nanospheres for nitrophenol explosives. Figure 2 showed the fluorescence spectra of hollow nanospheres in ethanol phase in the presence of different concentrations of TNP, NP and DNP. As shown in Figure 2(a), the fluorescence was almost completely quenched when the concentration of TNP in ethanol was only 17.5 μM. The linear Stern-Volmer curve is presented in Figure 2(b). The quenching constant (K_{sv}) was calculated to be 9.67×10^5 M^{-1}, and the LOD value for TNP was found to be 0.084 μM based on S/N=3 at lower concentrations of TNP. The fluorescence spectra of polymer hollow nanospheres upon the addition of NP also presented high quenching effect (Figure 2(c, d)). K_{sv} of hollow nanospheres for NP obtained from the linear fitting of plot was found to be 3.14×10^5 M^{-1} in the concentration range of NP 0–34.9 μM, and the detection limit was calculated to be 0.26 μM. In addition, DNP can also decrease the fluorescence intensity of the hollow spheres, and the quenching constant was calculated as 4.8×10^4 M^{-1} which is lower than that for TNP and NP (Figure 2(e, f)). It can be seen that the quenching response of TNP is the highest among nitrophenol explosives, while that of DNP is the lowest, due to the electron deficient nature of TNP based on the strong electron-withdrawing tendency of the substituted nitro groups [49,50]. It can also be seen in Figure 2(c, e) that the fluorescence peak of the polymer was redshifted from 441 to 461 nm with the increase of the concentration of NP which changed more than that of DNP. The obvious fluorescence peak location change indicates that the interaction between polymer and NP is stronger than that between polymer and DNP. Therefore, the fluorescence quenching effect of DNP is lower than that of TNP and NP [51]. At high concentration of

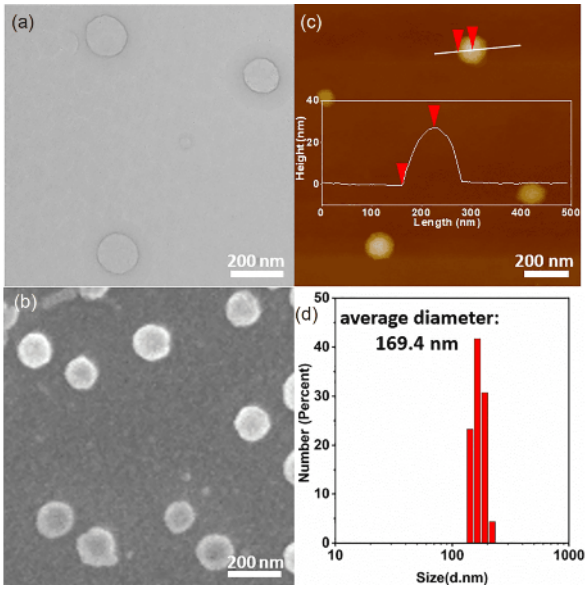

Figure 1 (a) TEM, (b) SEM and (c) AFM image of hollow spheres (inset: height profile along the line in the AFM of polymer hollow spheres). (d) Particle size distribution of hollow spheres (color online).

nitrophenol explosives, the Stern-Volmer quenching curves diverged from linearity and bended upward gradually with the increasing of nitrophenol explosives concentration, illustrating the super-amplified quenching effect (Figure 2(b, d, f)) [28,29,52]. Figure S9 demonstrated the fluorescence quenching of polymer hollow nanospheres in solution with the addition of nitrophenol explosives. The schematic representation of nitrophenol explosives detection by polymer hollow nanospheres was also shown in Scheme 1.

To evaluate the selectivity of hollow nanospheres, other nitroaromatics, 2,4-dinitrotoluene (DNT), 4-nitrotoluene

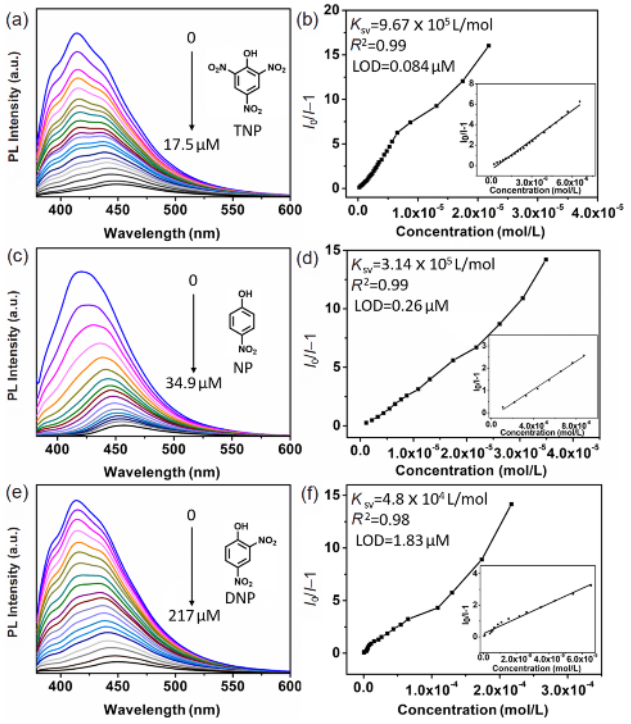

Figure 2 Fluorescence spectra of polymer HS in ethanol phase in the presence of different concentrations of (a) TNP, (c) NP and (e) DNP; the Stern-Volmer plots of ($I_0/I-1$) values versus the concentrations of (b) TNP, (d) NP and (f) DNP (inset: the enlarged Stern-Volmer plots at low concentrations of (b) TNP, (d) NP and (f) DNP) (color online).

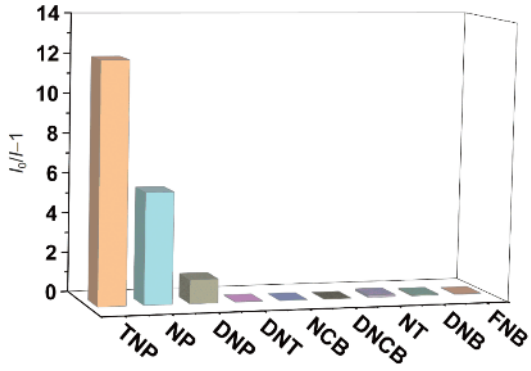

Figure 3 Changes in fluorescence intensity induced by different nitroaromatic analytes; the concentration of them is 17.5 μM (color online).

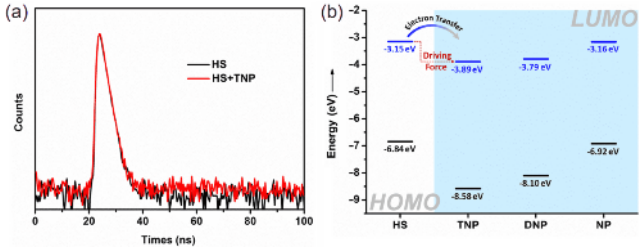

Figure 4 (a) Fluorescence decay curves of HS before and after adding TNP in ethanol solution. (b) Pictorial representation of excited state electron transfer from the LUMO of HS to the LUMO of nitrophenol explosives (color online).

(NT), 4-chloronitrobenzene (NCB), 2,4-dinitrochlorobenzene (DNCB), *m*-dinitrobezene (DNB), and *p*-nitrobenzaldehyde (FNB) whose molecular structure were shown in Figure S10, were added to the solution of the hollow nanospheres, respectively. Figure 3 showed the selectivity of the hollow nanospheres towards nitrophenol explosives, indicating that only the nitrophenol explosives (TNP, DNP and NP) significantly quenched the fluorescence emission of hollow spheres comparing with the analogous nitroaromatic compounds. The sensing ability of hollow nanospheres as well as other AIE-active covalent nanomaterials for nitrophenol explosives were summarized in Table S1 (Supporting Information online). The hollow nanospheres exhibited higher K_{sv} than other AIE-active covalent nanomaterials, indicating the potentiality of hollow nanospheres for the sensitive and selective detection of nitrophenol explosives.

3.3 Mechanism of sensing

To understand the origin of the sensitivity of hollow nanospheres towards nitrophenol explosives, the sensing mechanism was investigated. As shown in Figure 4(a) and Figure S11, the lifetime of the hollow nanospheres remains almost unchanged when adding nitrophenol explosives solution into the solution of HS, suggesting that the fluorescence quenching of the polymer hollow nanospheres mainly originated from a static mechanism [29,53–56]. Although the UV-Vis absorption spectra of nitrophenol compounds exhibited an overlapping with the fluorescence spectra of the hollow nanospheres (Figure S12), the unchanged lifetime of hollow spheres ruled out the possibility of the resonance energy transfer process. To assess the feasibility of PET from electron-rich polymer hollow nanospheres to electron-deficient nitrophenol analytes, we calculated the highest occupied molecular orbital (HOMO) and lowest occupied molecular orbital (LUMO) of the polymer hollow spheres and nitroaromatic compounds through cyclic voltammetry measurement (Figure 4(b), Figures S13, S14). The LUMO level of the polymer hollow spheres was calculated to be −3.15 eV, which is higher than that of nitrophenol explosives. The energy difference between the LUMO level of the donor fluorescence polymer hollow spheres and that of the accepter nitrophenol compounds provided thermodynamic driving force for the electron transfer from polymer hollow spheres to nitrophenol analytes, and then electrons came back to the ground state via a nonradiative process, resulting in the fluorescence quenching of polymer hollow spheres [52–58]. Notably, the LUMO energy of polymer HS was lower than the other nitroaromatic compounds, indicating that PET is the reason for the selective fluorescence quenching for nitrophenol explosives. Meanwhile, the den-

sity of states (DOS) was calculated by DFT to further confirm the PET process. The optimized structures of polymer hollow nanospheres were simulated and the optimal contact location of TNP on polymer hollow nanospheres was found at the outside phenyl ring of TFPB moiety (Figures S15, S16). Orbital analysis showed that the LUMO+2 was mostly concentrated on TFPB moiety of polymer hollow nanospheres, while the LUMO and LUMO+1 were predominantly distributed on TNP unit. Thus, the excited state level of polymer hollow nanospheres was higher than that of TNP, indicating the PET process from polymer hollow nanospheres to TNP (Figures S17, S18). To further investigate the origin of super-amplified quenching effect, we made a profound study of the interaction between TNP and the polymer HS. We used the MOE's builder tool to estimate the intermolecular interactions between the polymer HS and TNP, and the lowest energy complexes of HS/TNP were rendered as two-dimensional and three-dimensional styles (Figure S19). It can be clearly seen that forces between the polymer HS and TNP are mainly composed of H-bonding between the hydroxyl groups on TNP and the imine bond beside triphenylbenzene. Thus, the hydrogen bonding interactions between HS and TNP made the combination of them closer, resulting in the super-amplified quenching effect of the hollow nanospheres [59,60].

3.4 Sensing for TNP in solid state

In order to realize rapid, convenient and inexpensive sensing of explosives, portable paper-based detectors were fabricated by dipping the Whatman filter paper in the hollow spheres solution before drying them in the air. The filter paper was cut into portable test strips and various concentrations of TNP in ethanol solutions (10 μL) were dripped onto the papers. Then we can clearly see that the fluorescence intensity of the paper decreased gradually with the increase of TNP concentration and finally the emission almost quenched when the concentration reaches 10^{-3} M (Figure 5(a, b)). Figure 5(c) showed that the darkness of the test paper gradually appeared with the increase of TNP concentration due to the fluorescence quenching of the hollow nanopheres by TNP. The response level of paper strips for TNP was as low as 10^{-9} M. It can be clearly seen that no obvious fluorescence quenching was observed after the other nitroaromatic solutions being dripped on the HS-coated filter paper (Figure S20). Moreover, TNP sensing in vapor phase was also established. The paper was placed in the flask with saturated TNP vapor and the fluorescence was measured at different TNP vapor fumigation times. As shown in Figure S21, the fluorescence emission of the paper was significantly decreased after being fumed only 15 s under TNP atmosphere and completely quenched after two hours' fumigation. Although our test paper can only detect saturated TNP vapor at present, test strips for trace amounts of nitrophenol explosives can still be expected in the future by optimizing monomers and nanostructures of polymer hollow spheres. Therefore, the hollow nanospheres coated test strips displayed sensitive and rapid sensing of TNP in solution as well as the vapor phase, which has application prospect in sensing and detecting nitrophenol explosives.

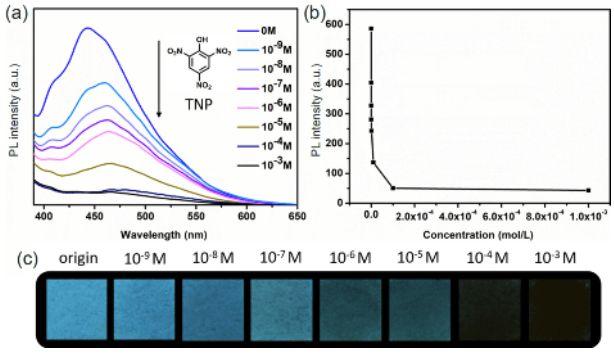

Figure 5 (a) Fluorescence spectra of the hollow spheres filter paper after adding different concentrations of TNP solutions. (b) The plot of the fluorescence intensity versus concentrations of TNP. (c) Fluorescent photographs of the hollow spheres filter paper upon TNP solutions with different concentrations (color online).

4 Conclusions

In summary, we prepared conjugated hollow nanospheres constructed by using AIE-active TFPB monomers for nitrophenol explosives sensing. The hollow nanospheres with bright blue emission in solution possessed high selectivity and sensitivity quenching response to nitrophenol explosives with K_{sv} of 9.67×10^5 M^{-1} for TNP and 3.14×10^5 M^{-1} for NP. The sensing mechanism can be attributed to photoinduced electron transfer process from polymer hollow nanospheres to nitrophenol explosives. In addition, a facile test strip was fabricated for the rapid detection of TNP with a low detection limit of 10^{-9} M. Our studies demonstrate that the hollow nanospheres can be used as an excellent sensor for nitrophenol explosives.

Acknowledgements This work was supported by the National Natural Science Foundation of China (21835001, 51773080, 21674041, 51573068, 21221063), Program for Changbaishan Scholars of Jilin Province, Jilin Province Project (20160101305JC), and the "Talents Cultivation Program" of Jilin University.

Conflict of interest The authors declare that they have no conflict of interest.

Supporting information The supporting information is available online at http://chem.scichina.com and http://link.springer.com/journal/11426. The supporting materials are published as submitted, without typesetting or editing. The responsibility for scientific accuracy and content remains entirely with the authors.

1 Lichtenstein A, Havivi E, Shacham R, Hahamy E, Leibovich R, Pevzner A, Krivitsky V, Davivi G, Presman I, Elnathan R, Engel Y, Flaxer E, Patolsky F. *Nat Commun*, 2014, 5: 4195
2 Wang DH, Cui YZ, Tao FR, Niu QF, Li TD, Xu H. *Sens Actuat B-Chem*, 2016, 225: 319–326
3 Wong MH, Giraldo JP, Kwak SY, Koman VB, Sinclair R, Lew TTS, Bisker G, Liu P, Strano MS. *Nat Mater*, 2017, 16: 264–272
4 Sodkhomkhum R, Masik M, Watchasit S, Suksai C, Boonmak J, Youngme S, Wanichacheva N, Ervithayasuporn V. *Sens Actuat B-Chem*, 2017, 245: 665–673
5 Gao K, Guo Y, Niu Q, Han L, Zhou L, Wang L. *Sens Actuat B-Chem*, 2018, 262: 298–305
6 Sylvia JM, Janni JA, Klein JD, Spencer KM. *Anal Chem*, 2000, 72: 5834–5840
7 Robert H, Prado PJ. *Appl Magn Reson*, 2004, 25: 395–410
8 Roscioli KM, Davis E, Siems WF, Mariano A, Su W, Guharay SK, Hill Jr. HH. *Anal Chem*, 2011, 83: 5965–5971
9 Harding G. *Radiat Phys Chem*, 2004, 71: 869–881
10 Engel Y, Elnathan R, Pevzner A, Davidi G, Flaxer E, Patolsky F. *Angew Chem Int Ed*, 2010, 49: 6830–6835
11 McQuade DT, Pullen AE, Swager TM. *Chem Rev*, 2000, 100: 2537–2574
12 Rose A, Zhu Z, Madigan CF, Swager TM, Bulović V. *Nature*, 2005, 434: 876–879
13 Hu Z, Deibert BJ, Li J. *Chem Soc Rev*, 2014, 43: 5815–5840
14 Chen Q, Cheng J, Wang J, Li L, Liu Z, Zhou X, You Y, Huang W. *Sci China Chem*, 2019, 62: 205–211
15 Li QY, Ma Z, Zhang WQ, Xu JL, Wei W, Lu H, Zhao X, Wang XJ. *Chem Commun*, 2016, 52: 11284–11287
16 Kumar V, Maiti B, Chini MK, De P, Satapathi S. *Sci Rep*, 2019, 9: 7269
17 Dalapati S, Jin E, Addicoat M, Heine T, Jiang D. *J Am Chem Soc*, 2016, 138: 5797–5800
18 Tawfik SM, Sharipov M, Kakhkhorov S, Elmasry MR, Lee YI. *Adv Sci*, 2019, 6: 1801467
19 Ma H, He C, Li X, Ablikim O, Zhang S, Zhang M. *Sens Actuat B-Chem*, 2016, 230: 746–752
20 Mei J, Leung NLC, Kwok RTK, Lam JWY, Tang BZ. *Chem Rev*, 2015, 115: 11718–11940
21 Kim HN, Guo Z, Zhu W, Yoon J, Tian H. *Chem Soc Rev*, 2011, 40: 79–93
22 Thomas SW, Joly GD, Swager TM. *Chem Rev*, 2007, 107: 1339–1386
23 Chen J, Xie Z, Lam JWY, Law CCW, Tang BZ. *Macromolecules*, 2003, 36: 1108–1117
24 Yuan WZ, Zhao H, Shen XY, Mahtab F, Lam JWY, Sun JZ, Tang BZ. *Macromolecules*, 2009, 42: 9400–9411
25 Chua MH, Zhou H, Lin TT, Wu J, Xu JW. *J Polym Sci Part A*, 2017, 55: 672–681
26 Liang G, Weng LT, Lam JWY, Qin W, Tang BZ. *ACS Macro Lett*, 2014, 3: 21–25
27 Zhou H, Li J, Chua MH, Yan H, Tang BZ, Xu J. *Polym Chem*, 2014, 5: 5628–5637
28 Chen T, Yin H, Chen ZQ, Zhang GF, Xie NH, Li C, Gong WL, Tang BZ, Zhu MQ. *Small*, 2016, 12: 6547–6552
29 Liu J, Zhong Y, Lu P, Hong Y, Lam JWY, Faisal M, Yu Y, Wong KS, Tang BZ. *Polym Chem*, 2010, 1: 426–429
30 Liu S, Jiang S, Xu J, Huang Z, Li F, Fan X, Luo Q, Tian W, Liu J, Xu B. *Macromol Rapid Commun*, 2019, 40: 1800892
31 Fan X, Tian R, Liu S, Qiao S, Luo Q, Yan T, Fu S, Zhang X, Xu J, Liu J. *Polym Chem*, 2018, 9: 1160–1163
32 Fan X, Tian R, Wang T, Liu S, Wang L, Xu J, Liu J, Ma M, Wu Z. *Nanoscale*, 2018, 10: 22155–22160
33 Baek K, Hwang I, Roy I, Shetty D, Kim K. *Acc Chem Res*, 2015, 48: 2221–2229
34 Pan L, Chortos A, Yu G, Wang Y, Isaacson S, Allen R, Shi Y, Dauskardt R, Bao Z. *Nat Commun*, 2014, 5: 3002
35 Guo CX, Li CM. *Phys Chem Chem Phys*, 2010, 12: 12153–12159
36 Huang KC, Hu CW, Tseng CY, Liu CY, Yeh MH, Wei HY, Wang CC, Vittal R, Chu CW, Ho KC. *J Mater Chem*, 2012, 22: 14727–14733
37 Li W, Zhang Q, Zheng G, Seh ZW, Yao H, Cui Y. *Nano Lett*, 2013, 13: 5534–5540
38 Li XL, Lou TJ, Sun XM, Li YD. *Inorg Chem*, 2004, 43: 5442–5449
39 Cheng Z, Dai Z, Li J, Wang H, Huang MR, Li XG, Liao Y. *Chem Eng J*, 2019, 357: 776–786
40 Das G, Skorjanc T, Sharma SK, Gándara F, Lusi M, Shankar Rao DS, Vimala S, Krishna Prasad S, Raya J, Han DS, Jagannathan R, Olsen JC, Trabolsi A. *J Am Chem Soc*, 2017, 139: 9558–9565
41 Wei Z, Wan M. *Adv Mater*, 2002, 14: 1314–1317
42 Hu M, Yang W, Liu S, Zhu W, Li Y, Hu B, Chen Z, Shen R, Cheong WC, Wang Y, Zhou K, Peng Q, Chen C, Li Y. *Chem Sci*, 2019, 10: 614–619
43 Wang Z, Lu P, Chen S, Gao Z, Shen F, Zhang W, Xu Y, Kwok HS, Ma Y. *J Mater Chem*, 2011, 21: 5451–5456
44 Wang B, Xie Z, Li Y, Yang Z, Chen L. *Macromolecules*, 2018, 51: 3443–3449
45 Taylor J, Brandbyge M, Stokbro K. *Phys Rev Lett*, 2002, 89: 138301
46 Perdew JP, Burke K, Ernzerhof M. *Phys Rev Lett*, 1996, 77: 3865–3868
47 Cheng J, Feng S, Han S, Zhang X, Chen Y, Zhou X, Wang R, Li X, Hu H, Zhang J. *ACS Nano*, 2016, 10: 9957–9973
48 Zhou X, Zhao Y, Chen S, Han S, Xu X, Guo J, Liu M, Che L, Li X, Zhang J. *Biomacromolecules*, 2016, 17: 2540–2554
49 Shanmugaraju S, Dabadie C, Byrne K, Savyasachi AJ, Umadevi D, Schmitt W, Kitchen JA, Gunnlaugsson T. *Chem Sci*, 2017, 8: 1535–1546
50 Feng HT, Zheng YS. *Chem Eur J*, 2014, 20: 195–201
51 Xiong S, Marin L, Duan L, Cheng X. *Carbohydr Polym*, 2019, 225: 115253
52 Zheng B, Li Y, Tao F, Cui Y, Li T. *Sens Actuat B-Chem*, 2017, 241: 357–363
53 Valeur B. *Molecular Fluorescence: Principles and Applications*. Weinheim: Wiley, 2005. 47
54 Lakowicz JR. *Principles of Fluorescence Spectroscopy*. New York: Springer, 2006. 48
55 Sohn H, Sailor MJ, Magde D, Trogler WC. *J Am Chem Soc*, 2003, 125: 3821–3830
56 Nagarkar SS, Joarder B, Chaudhari AK, Mukherjee S, Ghosh SK. *Angew Chem Int Ed*, 2013, 52: 2881–2885
57 Ma XS, Cui YZ, Ding YQ, Tao FR, Zheng B, Yu RH, Huang W. *Sens Actuat B-Chem*, 2017, 238: 48–57
58 Germain ME, Knapp MJ. *Chem Soc Rev*, 2009, 38: 2543–2555
59 Sun X, Wang Y, Lei Y. *Chem Soc Rev*, 2015, 44: 8019–8061
60 Tasci E, Aydin M, Gorur M, Gürek AG, Yilmaz F. *J Appl Polym Sci*, 2018, 135: 46310